Studies of molecular Rydberg states by Schwinger variational-quantum defect methods: Application to molecular hydrogen

J. A. Stephens and V. McKoy

Citation: The Journal of Chemical Physics **97**, 8060 (1992); doi: 10.1063/1.463428
View online: http://dx.doi.org/10.1063/1.463428
View Table of Contents: http://scitation.aip.org/content/aip/journal/jcp/97/11?ver=pdfcov
Published by the AIP Publishing

Studies of molecular Rydberg states by Schwinger variational-quantum defect methods: Application to molecular hydrogen

J. A. Stephens[a] and V. McKoy
Arthur Amos Noyes Laboratory of Chemical Physics,[b] California Institute of Technology, Pasadena, California 91125

(Received 3 August 1992; accepted 25 August 1992)

An *ab initio* electronic structure technique has been developed to study highly excited states of molecules by combining Schwinger variational methods of collision theory with generalized quantum defect theory. The technique exploits methods of scattering theory to study the region of highly excited Rydberg levels below and across ionization thresholds for molecules. The reaction matrix K, which describes the interaction of the Rydberg electron with the ionic core, is found at arbitrary negative electron energies by employing an unbounded Coulomb Green's function in the Lippmann–Schwinger equation for the electronic wave function. Quantal conditions are imposed to obtain discrete molecular energy levels, associated Rydberg wave functions, and quantum defect functions, all as a function of the internuclear distance. Results within the static-exchange approximation for the $^{1,3}\Sigma_u^+(1\sigma_g n\sigma_u)$ and $^{1,3}\Pi_u(1\sigma_g n\pi_u)$ Rydberg states of H_2, for $n=2$–20 and $R=1.2$–5.0 a_0, are presented and discussed.

I. INTRODUCTION

The study of the spectroscopy and electronic structure of atomic and molecular Rydberg states is inherently fundamental to their physics and chemistry, in all of its many-faceted aspects.[1–5] Much of our detailed information about Rydberg states of molecules in particular has been derived from single-photon, high-resolution photoabsorption and emission studies in the vacuum ultraviolet. Since the early 1980's new techniques of high-resolution laser spectroscopy have been developed and explored, which will continue in the forseeable future. These techniques include resonance enhanced multiphoton ionization,[6] which is effectively being coupled with high-resolution photoelectron spectroscopy,[7–12] including optical–optical[13–15] and microwave–optical[16] double-resonance spectroscopies, as well as zero-kinetic-energy (ZEKE) spectroscopy.[17] Sources of coherent, narrow-band, and tunable vacuum uv light for single-photon studies are also being developed.[18,19] These new experimental techniques are designed to prepare and investigate molecules in highly excited electronic states, very often Rydberg states, whose state densities become infinite below ionization thresholds due to the long-range Coulomb field outside the residual molecular ion core. The levels of excitation accessed in some current experiments, and those expected in the future, are such that their calculation from first principles using traditional quantum chemistry techniques based on direct diagonalization of Hamiltonian matrices becomes unfeasible. Fortunately, Rydberg states, their series, and their interaction with other (valence) electronic states may be largely characterized by a single parameter, the quantum defect μ. The quantum defect determines the deviation of the atomic or molecular ion core from that of a proton. For molecules, this parameter depends on both electron energy ϵ and molecular geometry, as emphasized by Mulliken nearly 30 years ago.[2] For a diatomic molecule with internuclear separation R we have then a quantum defect surface $\mu=\mu(\epsilon,R)$.

In this paper we discuss theoretical methods appropriate for determining the quantum defect surface, as well as the associated bound electronic states of molecular systems. This is accomplished by combining Schwinger variational and generalized quantum defect methods of electron–ion collision theory, which is outlined further below. Specifically we calculate the $^{1,3}\Sigma_u^+(1\sigma_g n\sigma_u)$ and $^{1,3}\Pi_u(1\sigma_g n\pi_u)$ Rydberg states, for $n=3$–20, over a range of internuclear distance spanning 1.2–5.0 bohr. The method allows calculation of Rydberg states to arbitrarily high principal quantum numbers. These calculations have been performed at the simplest level of the electron–ion interaction, namely, the Hartree–Fock static-exchange level. We expect that the static-exchange bound orbitals and quantum defect surface obtained by this method to be semiquantitatively useful in studies of single or multiphoton ionization, over internuclear distances ranging approximately 1 bohr unit about R_e of the H_2^+ ion. The limitations of the Hartree–Fock model at large internuclear distances are well known, and hence we cannot expect the present results to account for the avoided crossings and dissociation of the electronic states of H_2.

Schwinger variational and quantum defect methods have in common the concept of focusing on the short-range part of the electron–target interaction in terms of a phase shift, quantum defect, or reaction matrix. Multichannel quantum defect theory (MQDT) is the semianalytic theory which exploits the fundamental nature of μ, developed initially by Seaton for atoms,[20,21] and extended to molecules by Fano.[22,23] A review of the molecular theory and several applications has been given.[24] Briefly, the quantum

[a]Corresponding author. Address as of September 1, 1992: Joint Institute for Laboratory Astrophysics, University of Colorado, Boulder, Colorado 80309-0440.
[b]Contribution No. 8632.

 0021-9606/92/238060-16$06.00

defect μ describes the net, complicated electron–electron and electron–nuclear dynamics at short range, i.e., within a limited reaction zone. With this concept, and that of the frame transformation and of boundary conditions of scattering theory which specify the probability of an electron emerging from the reaction zone (or not, in the case of a bound state), MQDT has successfully accounted for many diverse and complicated photoabsorption and photoionization processes.[24] To date the most extensive applications of MQDT have relied on quantum defect parameters derived mainly from high-quality, high-resolution photoabsorption data. For molecules other than H_2, and to a lesser extent NO, the quantum defect surface is still virtually unexplored. There have been few systematic attempts to develop *ab initio* methods to calculate quantum defect surfaces. Shimamura *et al.*[25] have recently applied the R-matrix approach to calculate the complex quantum defects of doubly excited states of H_2, and successfully treated the avoided crossings and double-well structures in the manifold of $^1\Sigma_g^+$ states. In an unpublished thesis, Yoo[26] has adapted the noniterative eigenchannel R-matrix method[27–29] to treat the $^{1,3}\Sigma_u^+$ and $^{1,3}\Sigma_g^+$ excited states of H_2, including its doubly excited states. It is thus appropriate to further exploit first-principle approaches to the calculation of MQDT's basic parameters for molecules.

Schwinger variational methods have been extensively developed and employed to study electron–molecule scattering and molecular photoionization processes.[30–32] References 31 and 32 give comprehensive reviews of its applications to diatomics and small polyatomic molecular systems to 1986. An essential physical aspect of the method is that one needs to represent the electronic wave function only in regions of configuration space around the atom or molecule where the interaction potential is different from zero (e.g., electron–neutral scattering) or from a pure Coulomb field (electron–ion scattering or photoionization). The Schwinger variational method also provides a formalism by which one can extend scattering theory to the range of negative (bound) electron energies. The first application of the Schwinger variational principle[33,34] to potential scattering by Blatt and Jackson[35] discussed calculation of a bound state of a particle in a well (in this case the deuteron) by examining the pole of the scattering matrix. They indicated its connection with the scattering phase shift obtained by the Schwinger variational method, although not by methods discussed in the present paper. For bound states in electron–ion scattering, Maleki and Macek,[36,37] Zubarev,[38] and Domke[39] have discussed the formulation and general characteristics of the method. Maleki and Macek also studied the performance of the method in applications to an analytic, screened Coulomb potential. Important advances in the development and applications of the method to atomic systems have been made by Watson and coworkers.[40–43] In particular Goforth *et al.*[43] coupled the generalized QDT with the Schwinger variational method and were able to compute quantum defects and wavefunctions up to principal quantum number $n=30$ in the lithium isoelectronic series. In our work, we discuss this theoretical approach outlining its full adaptation to molecular systems.

The present paper discusses the eigenphase shifts (quantum defects) and total electronic energies (potential energy curves) obtained by diagonalizing the negative energy reaction matrix K of collision theory. Applications to molecular spectra, as well as incorporation of electronic multichannel interactions (e.g., two-electron excitations) is the subject of future work. A brief review of Schwinger variational theory applied to bound states, and formulation to obtain K and quantum defect parameters below threshold is discussed in Sec. II. Section III discusses numerical details, and its application to the Rydberg states of H_2 is discussed in Sec. IV. Section V gives a brief conclusion.

II. THEORY

A. Lippmann–Schwinger equation for bound states

The Lippmann–Schwinger equation for a bound state of an atom or molecule is[36–44]

$$|\Psi\rangle = -G_c V_s |\Psi\rangle, \tag{1}$$

where $V_s = V - V_c$ is the short-range interaction potential of the excited (Rydberg) electron with the core, with the pure Coulomb potential V_c removed. Here $G_c(\mathbf{r},\mathbf{r}')$ is the negative-energy Coulomb Green's function, which is bounded and decays exponentially at large electronic radial distance r. If a separable approximation to the short-range potential is made,

$$V_s^{\text{sep}} = V_s |\phi_t\rangle \langle \phi_t | V_s | \phi_t \rangle^{-1} \langle \phi_t | V_s, \tag{2}$$

where $|\phi_t\rangle$ is a trial wave function, an eigenvalue equation for the bound states results

$$\langle \phi_t | V_s + V_s G_c V_s | \phi_t \rangle = 0. \tag{3}$$

Maleki and Macek[36] and Watson[40] have demonstrated the variational property of Eq. (3). An equivalent set of homogeneous matrix equations, more amenable to numerical solution, is obtained by expanding the trial wave function in a basis $|u_i\rangle$. Square-integrable, Cartesian Gaussian functions have proven most convenient for molecules in continuum applications.[30–32] This is due to their flexibility, their computationally efficient re-expansions about a single center, and the relative ease in analytical evaluations of matrix elements of one- and two-electron operators in the potential V_s. We then have

$$|\phi_t\rangle = \sum_i c_i |u_i\rangle, \tag{4}$$

$$\sum_i \langle u_j | V_s + V_s G_c V_s | u_i \rangle c_i = 0. \tag{5}$$

Equation (5) implies that the determinant of the coefficient matrix $\langle u_j | V_s + V_s G_c V_s | u_i \rangle$ must vanish for a bound state. Having obtained the expansion coefficients c_i by solving Eq. (5) for a determined eigenvalue, the molecular Rydberg wave function, to within normalization, is then

$$|\Psi\rangle = -\sum_i c_i G_c V_s |u_i\rangle. \tag{6}$$

The above procedure requires a separate search for each energy eigenvalue of Eq. (3) or (5), which although it is stated to be rather laborious, has been implemented and used successfully for atoms.[40–44] The Coulomb Green's function G_c is also singular at the hydrogenic energies, but since it is known where these singularities occur, they can be avoided in the search procedure. For molecules, a separate search for many Rydberg states at many different internuclear distances may very well become prohibitive in effort and costs.

B. Negative energy reaction matrix

Generalized quantum defect theory[45,46] allows definition of a "smooth" reaction matrix K at all negative electron energies, i.e., not just at those for true bound levels. The Green's function needed to calculate this K matrix is free of singularities at hydrogenic poles, and is unbounded at large r. Here r is the radial distance between the electron and the molecular-ion center of mass. Using this Green's function, calculation of the reaction matrix as a continuous function of energy below threshold alleviates the need for a separate search for each eigenvalue in Eqs. (3) or (5). Goforth, Snitchler, and Watson[43] have successfully implemented this procedure in atomic systems.

The reaction matrix K, which at the simplest level in a molecule describes the coupling between alternative orbital angular momenta l of a Rydberg electron in the anisotropic molecular field, is given by the Schwinger variational expression

$$K_{l,l'm}=-\frac{1}{W_l}\sum_{i,j}\langle F_{lm}|V_s|u_i\rangle[f^{-1}]_{ij}\langle u_j|V_s|F_{l'm}\rangle, \tag{7}$$

where the matrix f_{ij} is

$$f_{ij}=\langle u_i|V_s+V_sG_c^sV_s|u_j\rangle. \tag{8}$$

Here $\langle \mathbf{r}|F_{lm}\rangle=f_l(r)Y_{lm}(\hat{r})/r$ are partial-wave components of regular Coulomb wave functions at negative energy, and $G_c^s(\mathbf{r},\mathbf{r}')$ is a smooth Green's function at negative energy, constructed[45] from regular and irregular Coulomb wave functions which lag each other by $\pi/2$ at large r. Explicitly,

$$G_c^s(\mathbf{r},\mathbf{r}')=-\sum_{l=0}^{\infty}\sum_{m=-l}^{m=+l}\frac{f_l(\epsilon,r_<)g_l(\epsilon,r_>)}{rr'}\times\frac{1}{W_l}Y_{lm}(\hat{r})Y_{lm}^*(\hat{r}'), \tag{9}$$

where in Eqs. (7) and (9) the Wronskian $W_l=f_lg_l'-f_l'g_l=2/\pi$ in atomic units, $r_<$ and $r_>$ denote the lesser and greater of r and r', and the pair (f_l,g_l) are the energy-normalized Coulomb wave functions.[45] Here the projection m specifies the spatial symmetry of the excited electron along the molecular axis, e.g., $m=0$ for σ and $m=\pm1$ for π orbitals. Equations (7)–(9) are appropriate for linear molecules. The basis functions $|u_i\rangle$ are equivalent to those used in the expansion of the trial wave function of Eq. (4). Use of Eq. (7) for the K matrix corresponds to solving the Lippmann–Schwinger equation, Eq. (1), for a separable potential of the form[31]

$$V_s^{\text{sep}}=\sum_{i,j}V_s|u_i\rangle[d^{-1}]_{ij}\langle u_j|V_s, \tag{10}$$

where the matrix $d_{ij}=\langle u_i|V_s|u_j\rangle$.

For Eqs. (7)–(9) to be applicable to molecular states, some additional specification of the Coulomb wave functions is required. The energy normalized wave functions we use are expressed in terms of Seaton's wave functions (f_l^0,g_l^0) which are analytic in the energy ϵ and related by the transformation,[21,45] for negative energies $\epsilon=-1/2\nu^2$ in a.u.,

$$\begin{aligned}f_l&=A^{1/2}f_l^0,\\ g_l&=A^{-1/2}\mathcal{G}f_l^0+A^{-1/2}g_l^0,\end{aligned} \tag{11}$$

and for positive energies $\epsilon=k^2/2=1/2\nu^2$ by

$$\begin{aligned}f_l&=B^{1/2}f_l^0,\\ g_l&=B^{-1/2}\mathcal{G}f_l^0+B^{-1/2}g_l^0.\end{aligned} \tag{12}$$

The coefficients A, B, and $\mathcal{G}$ depend on l and the energy parameter ν, and are given in Table I of Ref. 45. For $\epsilon<0$ the parameter $A=\Pi_{p=0}^{l}(1+\epsilon p^2)$ becomes negative for $\nu-l<0$ (i.e., for strongly closed channels), and f_l and g_l become imaginary.[47] In our procedure we redefine these functions in terms of real functions as $f_l=i\bar{f}_l$ and $g_l=-i\bar{g}_l$, which preserves both the value of the Wronskian W_l and G_c^s and $K_{l,l'm}$ defined above.

C. Quantum defect functions and potential energy curves

With a smooth reaction matrix defined at all negative energies ϵ, quantum defect functions at any energy are obtained by diagonalization of K at fixed internuclear distance R,

$$\tan[\pi\mu_{\alpha\Gamma}(\epsilon,R)]=\sum_{l,l'}U_{\alpha lm}^{-1}(R)K_{l,l'm}(R)U_{l'm\alpha}(R). \tag{13}$$

Here U is the matrix which diagonalizes K, α labels the eigenchannel, and Γ represents any other set of quantum numbers needed to specify the spatial symmetry and spin coupling of the Rydberg states. Equation (13) is the multichannel (in l) analog of the single-channel quantum defect μ_l or phase shift δ_l. For a spherically symmetrical (atomic) field Eq. (13) reduces to the quantum defect relationship

$$\mu_l(\epsilon)=\pi^{-1}\delta_l(\epsilon)=\pi^{-1}\arctan K_l(\epsilon). \tag{14}$$

Having obtained $\mu_{\alpha\Gamma}(\epsilon,R)$, over a fairly coarse grid in the energy, one may then accurately find the actual bound state energies by first fitting μ to a low-order power series in ϵ,

$$\mu_{\alpha\Gamma}(\epsilon,R)=\sum_{i=0}^{p}a_i\epsilon^i \tag{15}$$

and then finding the roots ϵ_n of the following equation, for a fixed integer n and eigenchannel index α

$$\mu_{\alpha\Gamma}(\epsilon,R)+n^*(\epsilon,R)-n=0. \tag{16}$$

Here $n^*(\epsilon,R) = 1/\sqrt{-2\epsilon(R)}$ is the effective quantum number at fixed R, and ϵ is given in atomic units. Note that the resulting energy eigenvalue depends implicitly on the internuclear distance.

With the eigenvalues and quantum defects obtained in this manner, the Rydberg wave functions with the correct asymptotic behavior may be constructed by numerical quadrature from the K matrix via[31,42,48] the Lippmann–Schwinger equation

$$|\phi\rangle = |F\rangle + G_c^s V_s|\phi\rangle = |F\rangle + G_c^s K|F\rangle, \tag{17}$$

where we have used the identity $V_s|\phi\rangle = K|F\rangle$. Note that Eq. (17) is equivalent in form to the Lippmann–Schwinger equation with an inhomogeneous term, i.e., it is identical to that solved for the continuum states. Beginning from Eq. (7) the procedure can be repeated in an iterative manner, using the functions from Eq. (17) as additional basis functions, with an expected rapid convergence of the eigenvalues, quantum defects, and wave functions, provided an adequate beginning basis $|u_i\rangle$ is employed. The converged quantum defect functions $\mu_{\alpha\Gamma}(\epsilon_n,R)$ then define a molecular Rydberg potential surface through

$$U_{n\alpha\Gamma}(R) = U^+(R) - \frac{1}{2[n-\mu_{\alpha\Gamma}(\epsilon_n,R)]^2}, \tag{18}$$

where $U_{n\alpha\Gamma}(R)$ is the potential energy of the neutral Rydberg state and $U^+(R)$ is the potential energy of the associated ion. The ion potential is amenable to direct calculation by standard bound-state quantum chemistry programs. It is also often available from standard parameterizations or RKR procedures which use experimentally determined constants.

III. COMPUTATIONAL DETAILS

A. Wave functions and potential

The present calculations have been performed in the frozen-core, static-exchange approximation to the electron–ion interaction. The electronic wave functions are of the form

$$\Psi(^{1,3}\Lambda) = \frac{1}{\sqrt{2}}\{|1\sigma_g\overline{\phi_\epsilon}| \pm |\overline{1\sigma_g}\phi_\epsilon|\}, \tag{19}$$

where the upper (lower) sign gives the triplet (singlet) wave function for the two-electron system, and we consider the Rydberg states with Σ_u and Π_u electronic symmetry ($\Lambda=0$ and 1). With these wave functions the static exchange, one-particle Schrödinger equation for the Rydberg orbital ϕ_ϵ is obtained from the variational expression, $\langle\delta\Psi|H-E|\Psi\rangle=0$, where H is the fixed-nuclei Hamiltonian and E is the total energy. Note that no boundary conditions specifying that $|\Psi\rangle$ is an actual bound state are required at this stage, so that this procedure is entirely equivalent to that used for the continuum.[30,31] The one-electron equation is of the form

$$P\left[f + \sum_i^{\text{core}} (2J_i - K_i) + J_n \pm K_n - \epsilon\right] P|\phi_\epsilon\rangle = 0, \tag{20}$$

where J_i and K_i are the Coulomb and exchange operators, and P is a projection operator which enforces orthogonality between the orbital of the excited electron and those in the ionic core. The one-electron operator in Eq. (20) is

$$f = -\frac{1}{2}\nabla^2 - \sum_\alpha \frac{Z_\alpha}{|\mathbf{r}-\mathbf{R}_\alpha|}, \tag{21}$$

where Z_α is a nuclear charge. For H_2, the projection operator is simply $P = 1 - |1\sigma_g\rangle\langle 1\sigma_g|$, and the short-range static-exchange potential is

$$V_s = J_{1\sigma_g}(\mathbf{r}) \pm K_{1\sigma_g}(\mathbf{r}) - \frac{1}{|\mathbf{r}-\mathbf{R}_1|} - \frac{1}{|\mathbf{r}-\mathbf{R}_2|}. \tag{22}$$

Note that numerically we usually work with a projected potential (generalized Phillips–Kleinman psuedopotential[30,31]), which includes both the static-exchange interaction and the constraint that the excited orbitals be orthogonal to those of the ionic core. In the present case they are orthogonal by symmetry.

We have used an iterative procedure,[30,31] based on the Schwinger variational principle, to solve Eq. (17), the Lippmann–Schwinger integral equation associated with Eq. (20). In this procedure, the static-exchange potential V_s is approximated by a separable form,

$$V_s^{\text{sep}}(\mathbf{r},\mathbf{r}') = \sum_{i,j} \langle\mathbf{r}|V_s|\alpha_i\rangle [V_s^{-1}]_{ij} \langle\alpha_j|V_s|\mathbf{r}'\rangle, \tag{23}$$

where the matrix V_s^{-1} is the inverse of the matrix with elements $(V_s)_{ij} = \langle\alpha_i|V_s|\alpha_j\rangle$ and the α's are discrete basis functions such as Cartesian or spherical Gaussian functions. With this approximation to V_s, the initial solution to Eq. (17) can be written

$$\phi^0_{\epsilon lm}(\mathbf{r}) = F_{\epsilon lm}(\mathbf{r}) + \sum_{i,j} \langle\mathbf{r}|G_c^s V_s|\alpha_i\rangle [D^{-1}]_{ij} \langle\alpha_j|V_s|F_{\epsilon lm}\rangle, \tag{24}$$

where

$$D_{ij} = \langle\alpha_i|V - VG_c^s V|\alpha_j\rangle. \tag{25}$$

The solutions obtained from Eq. (24) are then used to augment the initial basis $\{\langle\mathbf{r}|\alpha\rangle\}$, which is continued in an iterative manner. In this study two iterations provided well-converged solutions of Eq. (17) at all negative energies. With the converged solutions, the physical Rydberg wave functions are obtained by transformation from the $\{l,m\}$ to the eigenchannel representation,

$$\phi_{\epsilon_n\alpha}(\mathbf{r}) = \sum_{lm} U_{\alpha lm}(\epsilon_n)\phi_{\epsilon_n lm}(\mathbf{r}), \tag{26}$$

where the matrix elements $U_{\alpha lm}(\epsilon_n)$ are obtained from Eq. (13) using energy eigenvalues ϵ_n calculated from Eq. (16).

B. Basis sets and grids

The Gaussian basis sets used in the separable representation of the static-exchange potential [Eq. (23)] and the initial K matrix [Eq. (7)], included Cartesian Gaussian

TABLE I. Basis set used in the separable potential, Eq. (10).

Symmetry	Center	Type of Gaussian function[a]	Exponents
σ_u	H	Cartesian z	8.0, 4.0, 2.0, 1.0, 0.63, 0.20
			0.1, 0.05, 0.01, 0.005, 0.0025, 0.001
	Midpoint	Spherical $l=1$	1.50, 0.75, 0.30, 0.10, 0.01
		$l=3$	1.50, 0.75, 0.30, 0.01
		$l=5$	1.50, 0.75, 0.30, 0.10
π_u	H	Cartesian x	8.0, 4.0, 2.0, 1.0, 0.63, 0.2
			0.1, 0.05, 0.01, 0.005, 0.001
		xz	8.0, 4.0, 2.0, 1.0, 0.63, 0.2
			0.1, 0.05, 0.01, 0.005, 0.001
	Midpoint	Spherical $l=1$	1.50, 0.75, 0.30, 0.10, 0.01
		$l=3$	1.50, 0.75, 0.30, 0.01
		$l=5$	1.50, 0.75, 0.30, 0.10

[a]Cartesian Gaussian basis functions are defined as $\phi^{\alpha,l,m,n,\mathbf{A}}(\mathbf{r})=N(x-A_x)^l(y-A_y)^m(z-A_z)^n\exp(-\alpha|\mathbf{r}-\mathbf{A}|^2)$ and spherical Gaussian functions are defined as $\phi^{\alpha,l,m,\mathbf{A}}(\mathbf{r})=N|\mathbf{r}-\mathbf{A}|^l\exp(-\alpha|\mathbf{r}-\mathbf{A}|^2)Y_{lm}(\Omega_{\mathbf{r}-\mathbf{A}})$, with N the normalization constant.

functions centered on the nuclei and spherical Gaussian functions centered on the bond midpoint, and are listed in Table I. The $1\sigma_g$ core wave function for H_2^+ was obtained with the "g" atomic basis set of Guberman,[49] augmented with three d ($\alpha=0.08$, 0.032, and 0.018) functions on the nuclei. In Table II we compare our calculation of the electronic energy of H_2^+ in this Gaussian basis with the exact results of Bates *et al.*[50] for $R=1.2$–$5.0\ a_0$. A deviation of no more than 0.01 eV at any R is apparent, a consideration which will limit the absolute accuracy of the present calculations for the Rydberg states.

In these calculations, all matrix elements and functions were evaluated by employing single-center expansions about the center of mass. For converged results, the following parameters were used:

(i) maximum partial wave in the K matrix=7;

(ii) maximum partial wave expansion of bound orbitals in the direct potential=14;

(iii) maximum partial wave expansion of $1\sigma_g$ bound orbital in the exchange potential=14;

(iv) maximum partial wave expansion of $1/r_{12}$ in the direct and exchange terms=28 and 14, respectively;

(v) maximum partial wave expansion of the nuclear potential=28.

The extent of the radial integration grid varies in this calculation with the negative energies at which the K matrices were computed. This is necessary due to the divergence of the Green's function beyond the radial turning point $r\sim 2n^{*2}$, where n^* is the effective quantum number. The negative energy Coulomb functions (f_l^0, g_l^0) were computed using Seaton's subroutine,[51] and transformed to the energy normalized pair through Eqs. (11) and (12). For energies $\epsilon \geqslant -4.0$ eV, accumulation of the eigenphase in Eq. (7) due to the short-range potential was stabilized to ~ 1–3×10^{-3}, and to $\sim 1\times 10^{-2}$ for $\epsilon=-5.44$ eV, the lowest electron energy explicitly considered. The integration step sizes ranged from 0.005 to 0.08 a.u., up to a maximum distance of 21.8 a_0, and contained 470 radial points.

TABLE II. Total electronic energies of hydrogen molecular ion.

$R(a_0)$	$-E$(a.u.)[a]	$-E$(a.u.)[b]
1.20	0.528 416	0.528 972
1.40	0.569 604	0.569 979
1.60	0.590 626	0.590 930
1.80	0.599 954	0.600 254
2.00	0.602 316	0.602 625
2.20	0.600 498	0.600 835
2.40	0.596 204	0.596 543
2.60	0.590 498	0.590 835
2.80	0.584 051	0.584 352
3.00	0.577 298	0.577 557
3.50	0.560 684	0.560 859
4.00	0.545 962	0.546 080
4.50	0.533 823	0.533 986
5.00	0.524 286	0.524 420

[a]Present results obtained using the Gaussian basis set discussed in the text.

[b]Exact results of Ref. 50. The points at $R=3.5$ and 4.5 were interpolated from their tables.

IV. RESULTS AND DISCUSSION

A. Eigenphase parameters and quantum defect functions

Here we survey the static-exchange, eigenchannel phase shifts and quantum defect functions obtained from solutions of Eqs. (13)–(16) for the $\alpha=1$ ("$p\sigma_u$"), 2 ("$f\sigma_u$") eigenchannels of $^{1,3}\Sigma_u^+$ symmetry, and $\alpha=1$ ("$p\pi_u$"), 2 ("$f\pi_u$") eigenchannels of $^{1,3}\Pi_u$ symmetry. Figures 1 and 3 show the variation of $\mu_\alpha(\epsilon,R)$ with internuclear distance and electron energy, extending across the ionization threshold into the near continua. The indicated points at which the eigenphase was computed were simply chosen to represent these functions on a coarse mesh, and do not correspond to energy eigenvalues. Figures 2 and 4 show our calculated quantum defect functions $\mu_\alpha(\epsilon_n,R)$ for the $n=2$–5 discrete states ϵ_n plotted as functions of internuclear distance. The solid dots in these figures and the potential plots discussed below correspond to the mesh of internuclear distances given in Table II.

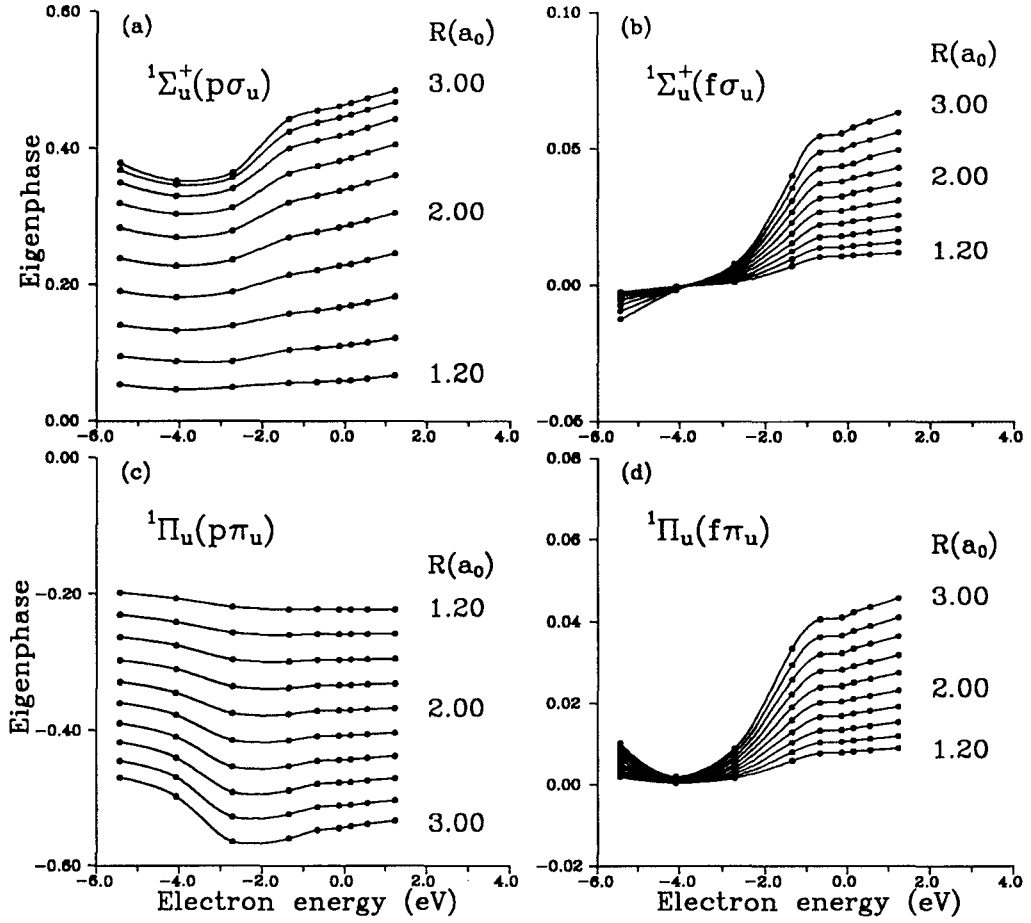

FIG. 1. Calculated eigenchannel phase shifts for $^1\Sigma_u^+$ and $^1\Pi_u$ symmetries in H_2, for $p\sigma_u$, $f\sigma_u$, $p\pi_u$, $f\pi_u$-type channels.

1. $^1\Sigma_u^+$ and $^1\Pi_u$ symmetries

Figure 1 shows the $^1\Sigma_u^+$ and $^1\Pi_u$ eigenphase parameters for eigenchannels $\alpha=1$ and 2 plotted as functions of electron energy. The relatively slow and smooth variation of these quantities with electron energy ϵ and R is apparent. These parameters compactly characterize the net interaction of the Rydberg electron with the ion core. Their smooth variation with the variables ϵ and R has served as a basic premise for the utility of the QDT. The continuity of the parameters across the ionization threshold also underscores the equivalence of electron–ion collision dynamics both in the near continua and in the region of discrete states just below threshold. This equivalence is manifest without regard to specific boundary conditions which determine the eventual outcome of the two-body collision.

The increase of eigenphase in the $^1\Sigma_u^+$ channel in Fig. 1(a) reflects evolution of $np\sigma_u$ levels to those with principal quantum number decreased by one unit, i.e., to a $(n-1)s$ orbital on one of the separated atoms. For a single electron orbital in the H_2^+ system this correlation from $R=0$ to $R=\infty$ and associated "electron promotion" is rigorous. However, the interaction with a second electron in neutral H_2 reduces this to only a pseudocorrelation.[2–4,52–54] The steplike behavior of the $f\sigma_u$ eigenchannel phase shifts in Fig. 1(b) (and all subsequent $\alpha=2$ channels) occurs because of the higher term values at which high angular momentum states must begin in the discrete spectrum.

Figure 2 shows our calculated quantum defect functions obtained for $^1\Sigma_u^+$ and $^1\Pi_u$ $n=2$–5 Rydberg states of H_2 in the static-exchange approximation. Plotted as functions of internuclear distance they reveal more clearly the effect of orbital promotion and restructuring of the ionic core as the system evolves from the united atom to separated atoms, with symmetry constraints imposed by the Wigner–Witmer rules. The rapid rise of eigenphase in the $^1\Sigma_u^+$ channel reveals the influence of promotion as R decreases, and the effect of avoided crossings with higher $^1\Sigma_u^+$ states at larger R, which prevents μ_α from rising by unity. For the first three members there is also significant energy dependence which increases with R. The $^1\Pi_u$ defects in Fig. 2(c) are less energy dependent due to smaller penetration of electron amplitude into the ion core. They are negative in phase, a peculiar effect Mulliken correctly attributed to cancellation of penetrational ($R=0$ united-atom ion field) and core splitting ($R\neq 0$ molecular-ion field) contributions to the $p\pi_u$ quantum defect in H_2.[4] Note that the $^1\Pi_u$ quantum defects show a dependence on R comparable in magnitude to the $^1\Sigma_u^+$ defects. As discussed below, this behavior underscores a basic deficiency of the

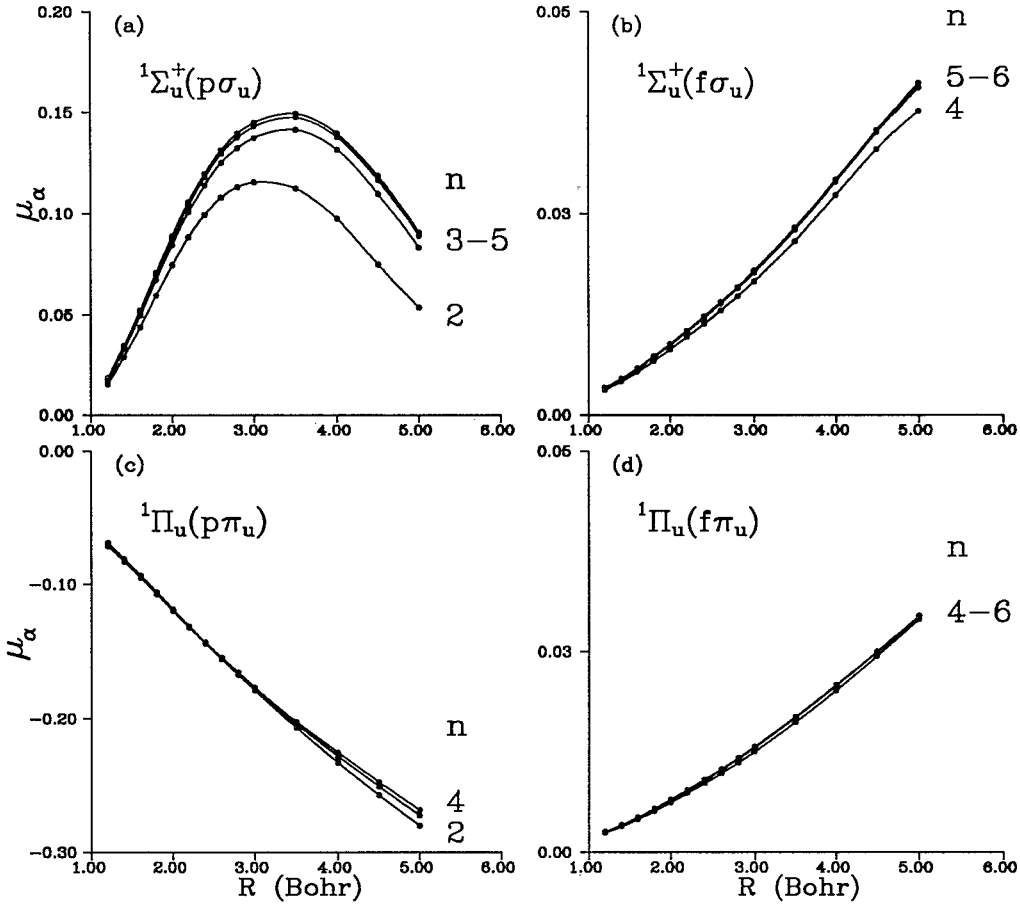

FIG. 2. Calculated quantum defect functions for $^1\Sigma_u^+$ and $^1\Pi_u$ Rydberg states in H_2, for $p\sigma_u$, $f\sigma_u$, $p\pi_u$, $f\pi_u$-type Rydberg states.

independent-electron approximation. The $f\sigma_u$ and $f\pi_u$ quantum defects are much smaller than the $p\sigma_u$ defects due to the small, but non-negligible, penetration of electron amplitude into the molecular core.

For positive electron energies, there have been several theoretical studies of low energy e^-–H_2^+ scattering which report the eigenphase sums for the channels presently investigated here.[55–59] Our computed eigenphase sums for both singlet and triplet symmetries treated here agree very well (e.g., within 0.001–0.005 rad) with values computed at low continuum energies at $R=2.0\ a_0$ of previous static-exchange studies.[55,56] Some studies have included polarization effects in the calculation of the e^-–H_2^+ continuum phase shifts, although l mixing induced by the nonspherical molecular field is not included in Ref. 57, and was treated perturbatively in the earlier work of Ref. 59. Polarization and l mixing is discussed further below regarding their role in bound regions of the spectrum and in comparing our quantum defect functions to the nearly exact ones available for molecular hydrogen.

2. $^3\Sigma_u^+$ and $^3\Pi_u$ symmetries

Figure 3 shows the $^3\Sigma_u^+$ and $^3\Pi_u$ eigenphase parameters for the eigenchannels $\alpha=1$ and 2. Generally the much larger eigenphase shift compared to singlet coupling reflects a reduced average potential energy of the excited electron when it is triplet coupled to the ion core, since the two-electron wave function Eq. (19) has a node at $\mathbf{r}_1=\mathbf{r}_2$. This of course gives rise to the usual singlet–triplet exchange splitting of these states, as seen in the computed potential energy curves presented below. Except for the $^3\Pi_u$ channel, the f-type eigenphases are all very similar in shape and magnitude to the singlets, due to the exceedingly small influence of electron exchange on these high-l states. The $^3\Pi_u$ eigenphases in Figs. 3(c) and 3(d) show a significant distortion as R increases, due to avoided crossings between the $\alpha=1,2$ eigenchannels, i.e., a strong p–f coupling of electron angular momenta occurs at larger internuclear distance.

Figure 4 shows the quantum defect functions obtained for $^3\Sigma_u^+$ and $^3\Pi_u$ Rydberg states of H_2 in the static-exchange approximation. We have not included the $n=2$ function in the $^3\Sigma_u^+$ channel, since the present numerical method cannot correctly determine this state beyond $R\sim2.2\ a_0$, where the $2p\sigma_u$ orbital evolves into the valence antibonding combination of hydrogen $1s$ orbitals. (Treatment of this true valence level at larger R requires implementation of the calculational framework discussed in Sec. II A.) The $^3\Pi_u$ quantum defect functions in Figs. 4(c) and 4(d) show more clearly the avoided crossing around $R\sim2.5\ a_0$.

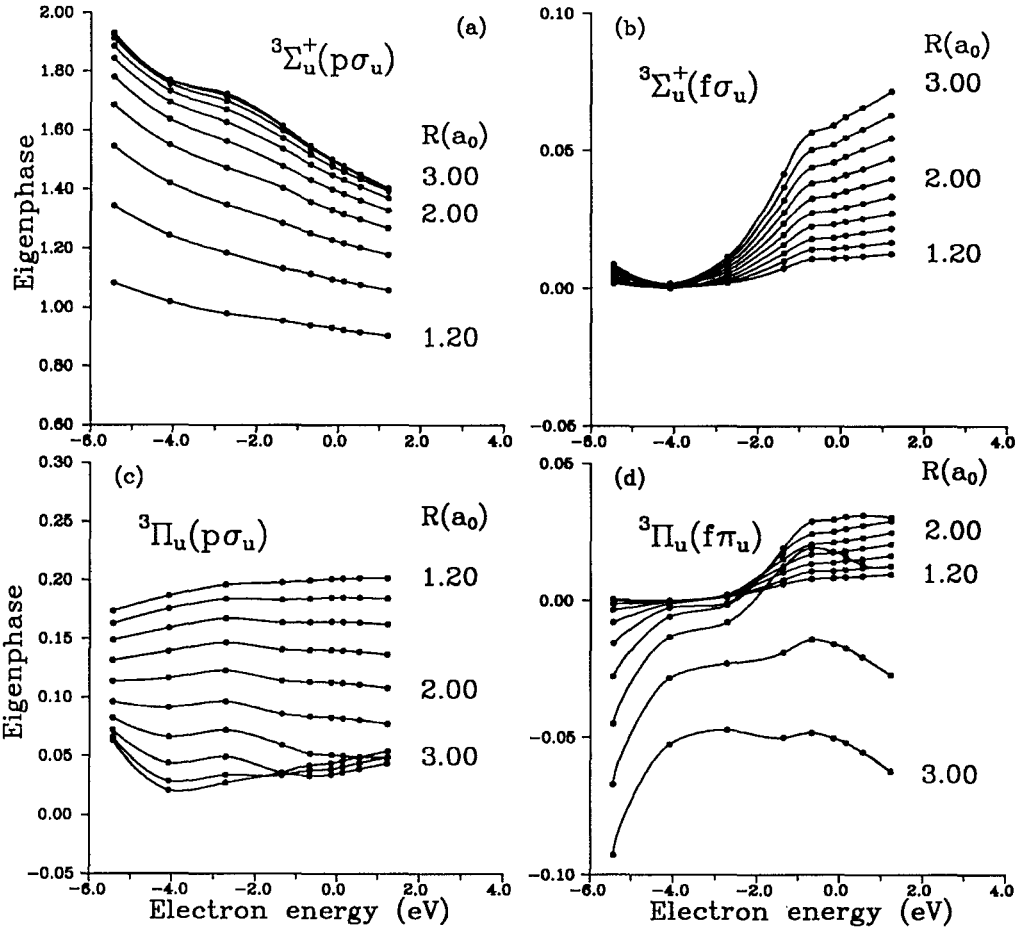

FIG. 3. Calculated eigenchannel phase shifts for $^3\Sigma_u^+$ and $^3\Pi_u$ symmetries in H_2, for $p\sigma_u$, $f\sigma_u$, $p\pi_u$, $f\pi_u$-type channels.

B. Comparison of quantum defect functions with other work

1. $^1\Sigma_u^+$ $np\sigma_u$ and $nf\sigma_u$ functions

In Fig. 5 we compare our calculated static-exchange quantum defect functions as functions of internuclear distance with those obtained from the very accurate Born–Oppenheimer potential curves which are available for some of the low-lying Rydberg states of H_2, as well as high-resolution photoabsorption experiments.[53,60,61] The latter can be considered essentially as exact, and have been employed in several quantitative applications of the MQDT to H_2. (The reader may consult Ref. 24 for a review of these applications.)

The difference between our computed curves and the exact ones fundamentally represents effects of electron correlations beyond electron exchange, the latter of which we treat exactly at the Hartree–Fock level. Note that in Figs. 5(a) and 5(b) the ordinate scale, or more precisely $-1/2(n-\mu_\alpha)^2$, represents a small portion of the total electronic energy. At $R\sim 2\ a_0$ and somewhat beyond this distance the wave functions obtained from the present method (and other one-electron methods at the same level of approximation, discussed below) already provides a quantitatively useful representation of the molecular excitations. The residual electron correlations we ignore play the dual role of inducing electronic polarization of the ion core by the outer electron, as well as insuring the molecule's dissociation into proper atomic products. The divergence of the $n>2$ quantum defect functions from the nearly exact values in Fig. 5 for $R>3\ a_0$ is due to incorrect dissociation limits of the wave function inherent in Eq. (19). This is simply the well-known deficiency of the molecular orbital method for even-electron homonuclear diatomics. Inclusion of Slater determinants of the form $|1\sigma_u n\pi_g|$ for $^{1,3}\Pi_u$ symmetry and $|1\sigma_u n\sigma_g|$ for $^{1,3}\Sigma_u$ symmetry as closed channels in a many-electron framework would reduce our Eq. (19) to the proper "linear-combination-of-atomic-substates" (LCAS) form at large R, as discussed by Mulliken.[3]

The $^1\Sigma_u^+(f\sigma_u)$ solid curve in Fig. 5(b) [as well as $^1\Pi_u(f\pi_u)$ in Fig. 6(b)] are the $\eta_l(\epsilon,R)$ defects[21] used to calculate the high-l energy levels of H_2 using the MQDT.[61] For $\epsilon=0$, they correspond to the μ_α quantum defects discussed here. We calculated these quantum defects explicitly for zero electron energy, and compare them in Fig. 5(b). We see that up to $R\sim 3\ a_0$, there is quite good agreement (the corresponding total energies agree to $\sim 10^{-4}$ a.u.), however beyond this the functions diverge, again owing to our one-electron approximation.

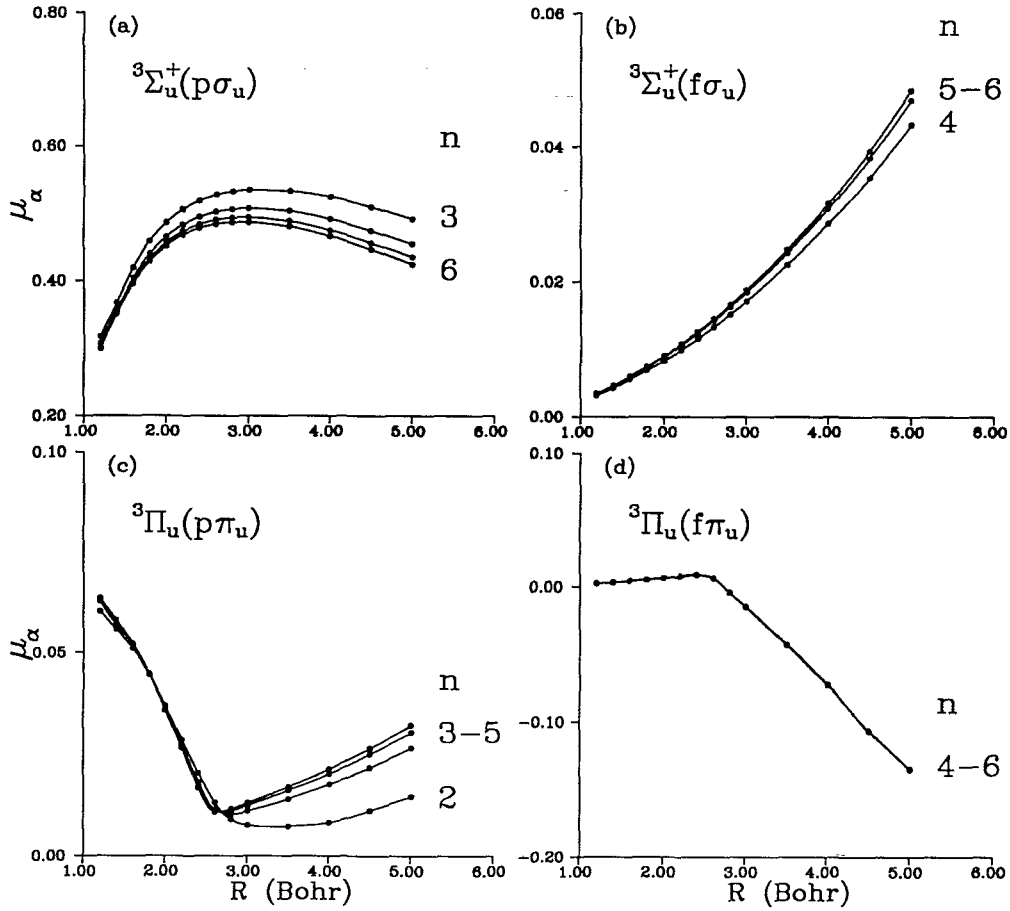

FIG. 4. Calculated quantum defect functions for $^3\Sigma_u^+$ and $^3\Pi_u$ Rydberg states in H_2, for $p\sigma_u$, $f\sigma_u$, $p\pi_u$, $f\pi_u$-type Rydberg states.

2. $^1\Pi_u$ $np\pi_u$ and $nf\pi_u$ functions

In Fig. 6 we compare our calculated static-exchange quantum defect functions as functions of internuclear distance with nearly exact functions for $^1\Pi_u$ Rydberg states. As for the $^1\Sigma_u^+$ states, we see comparable levels of agreement around $R\sim 2\ a_0$, with increasing discrepancy with the very accurate results as R increases. This again reflects the inability of a wavefunction of the form given by Eq. (19) to properly represent dissociation.

C. Born–Oppenheimer potential energy curves

1. $^1\Sigma_u^+$ and $^1\Pi_u$ states

In Fig. 7 we show our calculated Born–Oppenheimer potential energy curves for the $^1\Sigma_u^+$ and $^1\Pi_u$ states of H_2 obtained from Eq. (18) and the (calculated) quantum defect functions. Due to the weak binding of the Rydberg electron to the ionic core, the neutral Rydberg states are quite similar to the ion curve, one of the simplest properties of such states. On the other hand, subtle inward shifts of the potential minima are correctly reproduced as the excitation increases from $n=2$ to $n=5$. Introduction of polarization interactions in a multichannel-scattering-theoretic framework will lower the total energies relative to these curves, as would a quantum-chemical treatment of configuration interaction. However, the latter method becomes increasing unfeasible as the excitation energy increases. Inclusion of two-electron excitations introduces "two-well" character to lower states at larger internuclear distance, concurrently giving the correct dissociation of these Rydberg states of the molecule.

2. $^3\Sigma_u^+$ and $^3\Pi_u$ states

Figure 8 shows calculated static-exchange potential energy curves for the triplet ungerade states of H_2 obtained from our quantum defect functions. We have not included the $b\ ^3\Sigma_u^+$ repulsive state, for reasons discussed earlier.[62] At $R\leqslant 2.0\ a_0$ we note that our calculations for the $^1\Pi_u$ and $^3\Pi_u$ states correctly reflect the structure of the associated united atoms, ortho- and para-helium, respectively. As R increases, however, a strictly molecular field effect occurs since the $^3\Pi_u(4f\pi_u)$ level must cross the $(4p\pi_u)$ level in a diabatic correlation to properly dissociate to $H(3d)+H(1s)$ atomic products. The present calculations shown in Fig. 7(b) predict this interaction to occur with 50–50 mixing of these states at $R\sim 2.5\ a_0$.

In Fig. 9 we show in detail the avoided crossing of the $4p\pi_u$ and $4f\pi_u$ quantum defect functions which leads to the avoided crossing in the potential energy curves. The interaction and avoided crossing continue up to and across the ionization threshold, and their occurence could be detected by multiresonant optical spectroscopy techniques. In par-

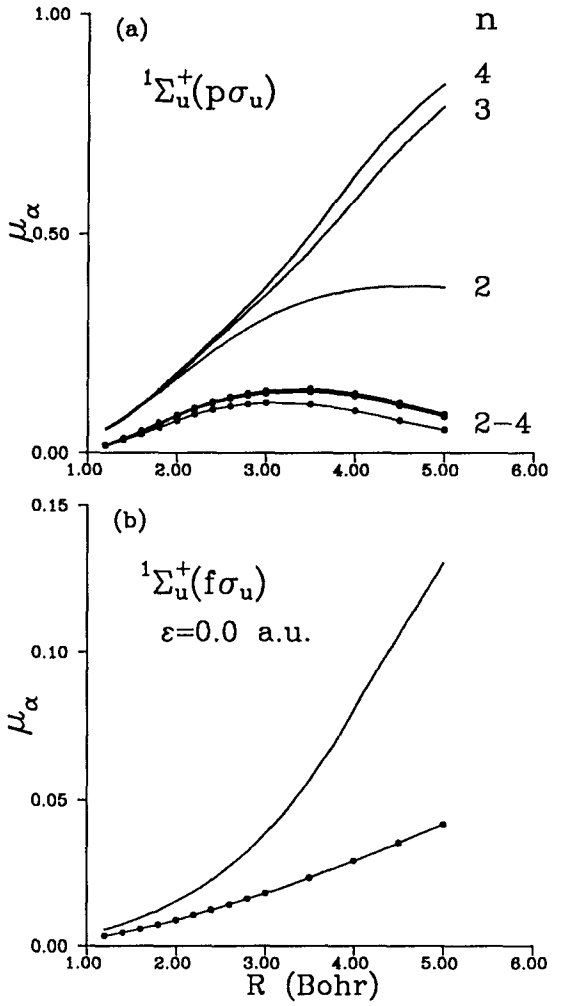

FIG. 5. Calculated quantum defect functions for $^1\Sigma_u^+$ Rydberg states in H_2, compared with nearly exact quantum defect functions from Ref. 53 ($p\sigma_u$) and 61 ($f\sigma_u$).

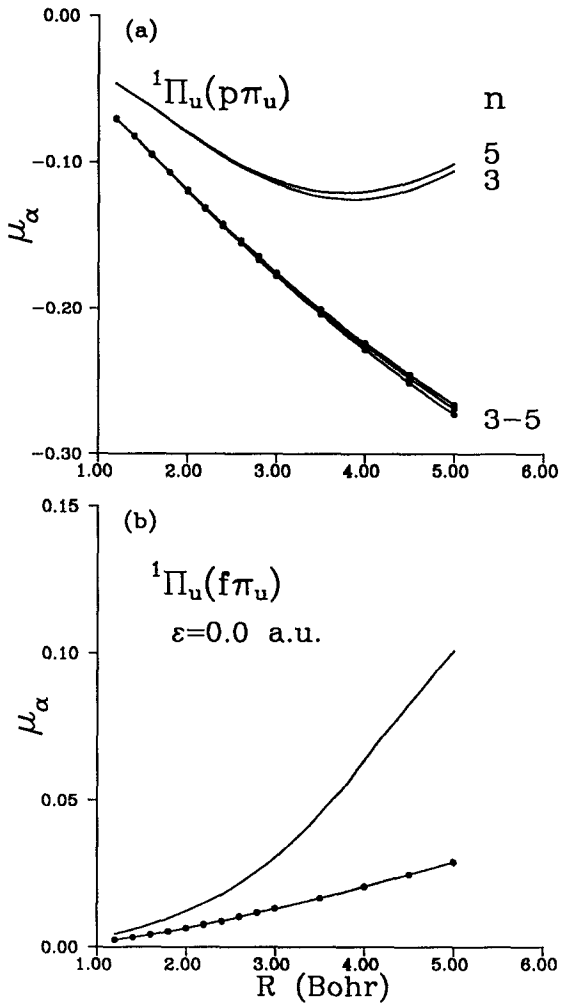

FIG. 6. Calculated quantum defect functions for $^1\Pi_u$ Rydberg states in H_2, compared with nearly exact quantum defect functions from Ref. 53, 60 ($p\sigma_u$), and 61 ($f\sigma_u$).

ticular, Eyler *et al.*[63] have actually observed several triplet $f\pi_u$ states in molecular hydrogen, for $n=10$–19. Preparing such Rydberg states with vibrational quanta $v=1$–3 and observing their rotationally resolved photoelectron spectra would indicate the influence of this strong l-mixing effect, and to what extent it is correctly described in a one-electron framework.

3. Comparison of total electronic energies with other results

In Table III we compare some numerical results for the total electronic energies for $^{1,3}\Sigma_u^+$ and $^{1,3}\Pi_u$ states of H_2 at the internuclear distance $R=2.0\ a_0$, computed at several levels of sophistication. First, we compare electronic energies calculated with the Schwinger variational-quantum defect method developed here with one-electron results we obtained using quantum-chemistry techniques. We have arbitrarily terminated our eigenvalue determination at the principal quantum number $n=20$. For each electronic symmetry considered, we also employed the "improved virtual orbital" (IVO) method[64,65] to determine the lower states, using the same Gaussian basis for H_2^+ discussed in Sec. III. The IVO energies result from a diagonalization of the Hamiltonian matrix within the independent electron approximation, and employ a frozen $1\sigma_g$ orbital of the ion. For low electronic excitation this method and the present approach should yield results in good agreement. Columns one and two compare these results, and our Schwinger variational-quantum defect approach reproduces the total electronic energy to within 0.001 a.u. for the $n=2$ and 3 states. For higher n, results from the IVO calculation rapidly deteriorate due to basis set deficiency, particularly for the $4p$ and $4f$ states. Column three also shows our computed self-consistent-field (SCF) Hartree–Fock total energies for each state using the same Gaussian basis. This calculation indicates the extent of relaxation of the $1\sigma_g$ core orbital from that of the pure ion. This effect is naturally largest for the $n=2$ $^{1,3}\Sigma_u^+$ states which have considerable valence character. The orbital relaxation is smaller in the $^{1,3}\Pi_u$ states and our results are in good agreement with the SCF results as well.

Second, we can now compare these one-electron results

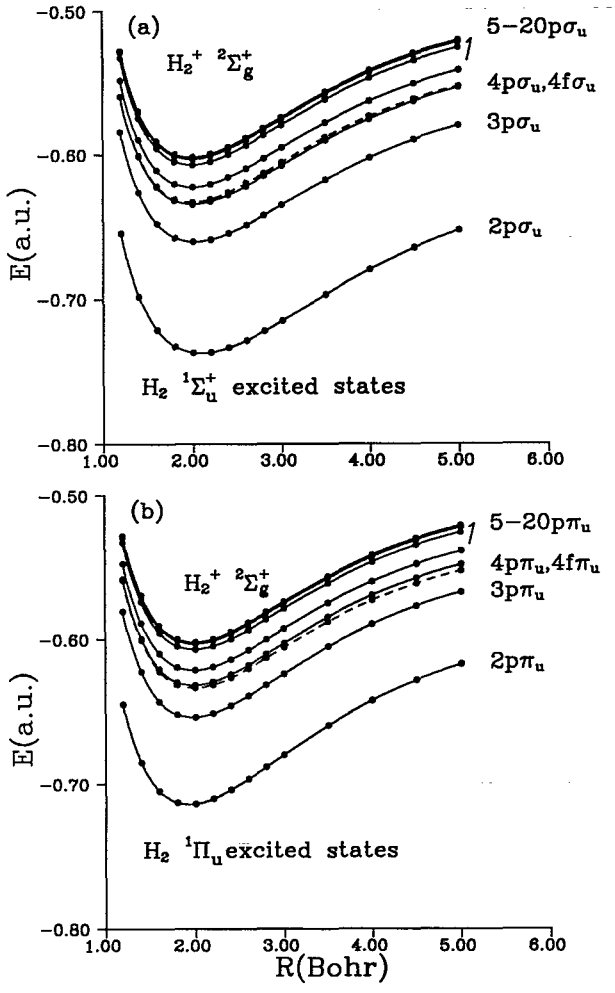

FIG. 7. Calculated potential energy curves for $^1\Sigma_u^+$ and $^1\Pi_u$ Rydberg states in H_2. The dashed line indicates the potential energy curve for the $^1\Pi_u$ ($1\sigma_g 4f\pi_u$) Rydberg state. The $n=20$ Rydberg states are indiscernible from the ion potential curve on this scale.

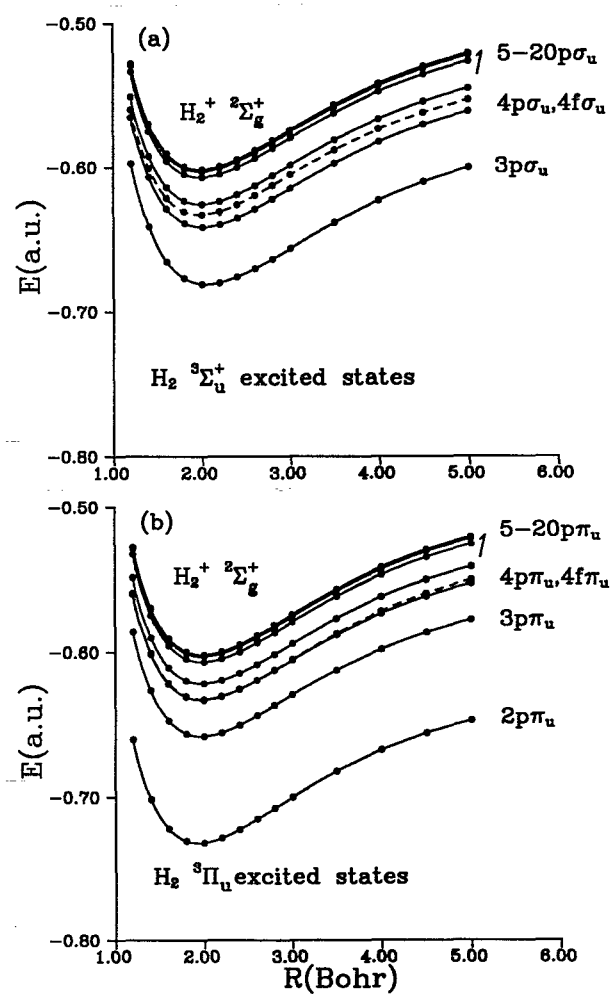

FIG. 8. Calculated potential energy curves for $^3\Sigma_u^+$ and $^3\Pi_u$ Rydberg states in H_2. The dashed line indicates the potential energy curve for the $^3\Pi_u$ ($1\sigma_g 4f\pi_u$) Rydberg state, although beyond $\sim 2.5\ a_0$, it undergoes an avoided crossing with the $^3\Pi_u$ ($1\sigma_g 4p\pi_u$) state. The $n=20$ Rydberg states are indiscernable from the ion potential curve on this scale.

with high-quality configuration-interaction calculations. These include the results of Rothenberg and Davidson[66] who examined the first several states of $^{1,3}\Sigma_u^+$ and $^{1,3}\Pi_u$ symmetry using the natural orbital configuration expansion, and the results of extensive studies by Kolos *et al.*[67–70] using generalized James–Coolidge-type wave functions. We also include the recent *ab initio* results of Wolniewicz and Dressler[71] at $R=2.0\ a_0$, since they also studied the higher $4f$ and $5p$ states of $^1\Sigma_u^+$ symmetry for the first time. For $n \leqslant 3$ the difference between results of Ref. 66–71 and our own reflects our neglect of electron correlation beyond the static-exchange level, similar to the comparison of the quantum defect functions above. For $n>3$, however, our Schwinger variational-quantum defect results agree quite well with these sophisticated calculations, where the IVO calculation fails due to basis set deficiency. In fact, for the IVO states with $n \geqslant 4$ in Table III, the virial ratio $-2\overline{T}/\overline{V}$ deviates considerably from unity, due to an inaccurate representation of the kinetic energy operator in the Gaussian basis. Our total energies are also somewhat lower at $R=2.0\ a_0$ for the $4f\sigma_u$ and $5p\sigma_u$ states compared to those of

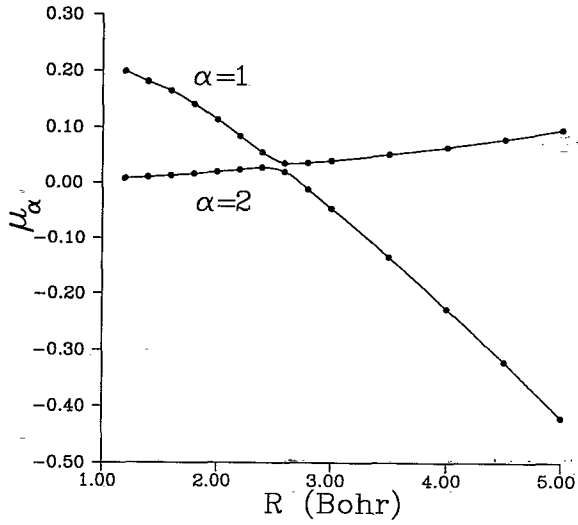

FIG. 9. Below threshold $\alpha=1$ ($p\pi_u$) and $\alpha=2$ ($f\pi_u$) quantum defects curves which undergo the avoided crossing.

TABLE III. Total electronic energies $-E$ of hydrogen molecule at $R=2.0\ a_0$. Energies are in units of a.u.

Symmetry	Present	IVO[a]	SCF[a]	Ref. 66	Refs. 67–70[c]	Ref. 71
$^1\Sigma_u^+$						
$1\sigma_g 2p\sigma_u$	0.737 821	0.738 569	0.740 528	0.750 402	0.752 054[(1)]	0.752 080
$1\sigma_g 3p\sigma_u$	0.661 306	0.661 382		0.664 922	0.665 441[(2)]	0.665 476
$1\sigma_g 4p\sigma_u$	0.635 044	0.632 710			0.636 866[(2)]	0.636 653
$1\sigma_g 4f\sigma_u$	0.633 698[b]	0.619 434				0.631 725
$1\sigma_g 5p\sigma_u$	0.623 077					0.620 762
$1\sigma_g 10p\sigma_u$	0.607 411					
$1\sigma_g 20p\sigma_u$	0.603 578					
$^3\Sigma_u^+$						
$1\sigma_g 2p\sigma_u$	0.881 957	0.883 351	0.892 675	0.896 697	0.897 064[(3)]	
$1\sigma_g 3p\sigma_u$	0.681 385	0.681 693		0.682 866		
$1\sigma_g 4p\sigma_u$	0.642 351	0.641 707				
$1\sigma_g 4f\sigma_u$	0.633 699[b]	0.624 902				
$1\sigma_g 5p\sigma_u$	0.626 565					
$1\sigma_g 10p\sigma_u$	0.607 800					
$1\sigma_g 20p\sigma_u$	0.603 624					
$^1\Pi_u$						
$1\sigma_g 2p\pi_u$	0.713 866	0.713 153	0.713 283	0.717 832	0.718 238[(4)]	0.718 241
$1\sigma_g 3p\pi_u$	0.653 641	0.653 220		0.655 035	0.655 230[(4)]	0.655 326
$1\sigma_g 4f\pi_u$	0.633 665[b]	0.624 690		0.633 939		
$1\sigma_g 4p\pi_u$	0.631 759	0.612 842		0.632 391		
$1\sigma_g 5p\pi_u$	0.621 386					
$1\sigma_g 10p\pi_u$	0.607 199					
$1\sigma_g 20p\pi_u$	0.603 551					
$^3\Pi_u$						
$1\sigma_g 2p\pi_u$	0.732 071	0.731 577	0.732 383	0.736 849		
$1\sigma_g 3p\pi_u$	0.659 252	0.659 027		0.660 233		
$1\sigma_g 4p\pi_u$	0.634 141	0.625 030		0.634 470		
$1\sigma_g 4f\pi_u$	0.633 667[b]	0.621 131		0.633 940		
$1\sigma_g 5p\pi_u$	0.622 608					
$1\sigma_g 10p\pi_u$	0.607 352					
$1\sigma_g 20p\pi_u$	0.603 571					

[a]Present results obtained using the Gaussian basis set described in the text.
[b]The calculated singlet–triplet splitting for these states is 0.2–0.4 cm^{-1}. Singlet–triplet splittings of the $4f\pi_u$ states observed in Ref. 61 were reported to be on the order of 0.05 cm^{-1}.
[c](1) Reference 67;(2) Ref. 68;(3) Ref. 69;(4) Ref. 70.

Wolneiwicz and Dressler.[71] For these levels, the inherent avoidance of convergence error due to basis set deficiency in our method outweighs inclusion of contributions from the correlation energy near the potential minima for these higher levels. On the other hand, we have not included the electron correlations which are essential to correctly describe these states and their avoided crossings ~ 5–$6\ a_0$.[68,71,72]

In the present approach based on the Lippmann–Schwinger equation, the full spectral representation of the Green's function $(E-H_0)^{-1}$ is used, and the kinetic energy operator is not approximated by matrix diagonalization methods such as the IVO approach. The present approach always treats the kinetic energy operator for the excited electron *exactly*, for states of arbitrary excitation, through use of the Coulomb Green's function in Eqs. (8) and (9). This advantage of the Schwinger variational principle over the Rayleigh–Ritz principle for bound state problems (the latter of which considers the full Hamiltonian in its variational functional) has been briefly discussed by Zubarev[38] and Watson.[44] At the outset we therefore implicitly include an infinite superposition of hydrogenic states in the description of the bound Rydberg electron.

V. CONCLUSION

We have discussed a method of electronic structure calculation particularly suited to the description of highly excited molecular electronic states. The application to the Rydberg states of molecular hydrogen, even at the present level of the independent-electron approximation, shows it to be an effective approach to situations where traditional quantum-chemical methods are physically and numerically inappropriate. Future work will include studies of the electronic wave functions and transition moments obtained by this method, and more importantly, their use in actual applications to the spectroscopy of electronically highly excited molecules. Extensions to other molecular systems and multichannel electronic interactions are also clearly needed.

ACKNOWLEDGMENTS

Work at the California Institute of Technology was supported by grants from the National Science Foundation, Air Force Office of Scientific Research, and the Office of Health and Environmental Research of the U.S. Department of Energy. We acknowledge use of resources of the JPL/Caltech CRAY Y-MP2E/116 Supercomputer. We thank Dr. Christian Jungen for many helpful discussions, suggestions, and interest in this work, as well as for providing the unpublished quantum defect functions from Ref. 61. Travel support for this research was provided by NSF INT-9016221, and a visiting fellowship given to J.A.S. from the C.N.R.S. in the fall of 1990. Thanks are due to Dr. Mireille Aymar for providing subroutines which calculate negative energy Coulomb wave functions. J.A.S thanks Professor Chris Greene for helpful discussions and interest in this research, and Dr. Steve Pratt for pointing out Ref. 71. J.A.S. also thanks Dr. Catherine Brechignac and Dr. Michel Gaillard, and the staffs of Laboratoire Aimé Cotton and Laboratorie Photophysique Moléculaire for their hospitality during visits where portions of this research was completed.

[1] S. Feneuille and P. Jacquinot, Adv. At. Mol. Phys. **17**, 99 (1981).
[2] R. S. Mulliken, J. Am. Chem. Soc. **86**, 3183 (1964).
[3] R. S. Mulliken, J. Am. Chem. Soc. **88**, 1849 (1966).
[4] R. S. Mulliken, J. Am. Chem. Soc. **91**, 4615 (1969).
[5] G. Herzberg, Annu. Rev. Phys. Chem. **38**, 27 (1987).
[6] P. M. Johnson and C. E. Otis, Annu. Rev. Phys. Chem. **32**, 139 (1981).
[7] R. N. Compton and J. C. Miller, in *Laser Applications in Physical Chemistry*, edited by D. K. Evans (Dekker, New York, 1989).
[8] P. M. Dehmer, J. L. Dehmer, and S. T. Pratt, Comments At. Mol. Phys. **19**, 205 (1987).
[9] K. Kimura, Adv. Chem. Phys. **60**, 161 (1985).
[10] J. P. Reilly, Isr. J. Chem. **24**, 266 (1984).
[11] W. A. Chupka, J. Chem. Phys. **87**, 1488 (1987).
[12] J. W. J. Verschuur and H. B. van Linden van den Heuvell, Chem. Phys. **129**, 1 (1989).
[13] W. Y. Cheung, W. A. Chupka, S. D. Colson, D. Gauyacq, P. Avouris, and J. J. Wynne, J. Phys. Chem. **90**, 1086 (1986).
[14] A. H. Kung, R. H. Page, R. J. Larkin, Y. R. Shen, and Y. T. Lee, Phys. Rev. Lett. **56**, 328 (1986).
[15] S. Fredin, D. Gauyacq, M. Horani, Ch. Jungen, G. Lefevre, and F. Masnou-Seeuws, Mol. Phys. **60**, 825 (1987).
[16] W. G. Sturrus, E. A. Hessels, P. W. Arcuni, and S. R. Lundeen, Phys. Rev. Lett. **61**, 2320 (1988).
[17] K. Müller-Dethlefs and E. W. Schlag, Annu. Rev. Phys. Chem. **42**, 109 (1991).
[18] T. P. Softley, W. E. Ernst, L. M. Tashiro, and R. N. Zare, Chem. Phys. **116**, 299 (1987).
[19] R. G. Tonkyn, J. W. Winniczek, and M. G. White, J. Chem. Phys. **91**, 6632 (1989).
[20] M. J. Seaton, Proc. Phys. Soc. **88**, 801 (1966).
[21] M. J. Seaton, Rep. Prog. Phys. **46**, 167 (1983).
[22] U. Fano, Phys. Rev. A **2**, 353 (1970).
[23] U. Fano, Comments At. Mol. Phys. **13**, 157 (1983).
[24] C. Greene and Ch. Jungen, Adv. At. Mol. Phys. **21**, 51 (1985).
[25] I. Shimamura, C. J. Noble, and P. G. Burke, Phys. Rev. A **41**, 3545 (1990).
[26] B. Yoo, Ph. D. thesis, Dept. of Physics, Louisiana State University, 1990 (unpublished).
[27] C. H. Greene, Phys. Rev. A **28**, 2209 (1983).
[28] H. Le Rouzo and G. Raseev, Phys. Rev. A **29**, 3338 (1984).
[29] C. H. Greene and L. Kim, Phys. Rev. A **38**, 5953 (1988).
[30] R. R. Lucchese, G. Raseev, and V. McKoy, Phys. Rev. A **25**, 2572 (1982).
[31] R. R. Lucchese, K. Takatsuka, and V. McKoy, Phys. Rep. **131**, 147 (1986).
[32] V. McKoy, S. N. Dixit, R. L. Dubs, and D. L. Lynch, Aust. J. Phys. **39**, 761 (1986).
[33] J. Schwinger, Phys. Rev. **72**, 742 (1947).
[34] B. A. Lippmann and J. Schwinger, Phys. Rev. **79**, 469 (1950).
[35] J. M. Blatt and J. D. Jackson, Phys. Rev. **26**, 18 (1949).
[36] N. Maleki and J. Macek, Phys. Rev. A **21**, 1403 (1980).
[37] N. Maleki, Phys. Rev. A **26**, 644 (1982).
[38] A. L. Zubarev, Sov. J. Part. Nucl. Phys. **9**, 188 (1978).
[39] W. Domke, J. Phys. B **15**, 2675 (1982).
[40] D. K. Watson, Phys. Rev. A **28**, 40 (1983).
[41] D. K. Watson, Phys. Rev. A **29**, 558 (1984).
[42] G. L. Snitchler and D. K. Watson, J. Phys. B **19**, 259 (1986).
[43] T. L. Goforth, G. L. Snitchler, and D. K. Watson, Phys. Rev. A **35**, 904 (1987).
[44] D. K. Watson, Adv. At. Mol. Phys. **25**, 221 (1988).
[45] C. Greene, U. Fano, and G. Strinati, Phys. Rev. A **19**, 1485 (1979).
[46] C. Greene, A. R. P. Rau, and U. Fano, Phys. Rev. A **26**, 2441 (1982).
[47] C. Greene, Phys. Rev. A **20**, 656 (1979).
[48] A. W. Fliflet and V. McKoy, Phys. Rev. A **18**, 2107 (1978).
[49] S. L. Guberman, J. Chem. Phys. **78**, 1404 (1983).
[50] D. R. Bates, K. Ledsham, and A. L. Stewart, Proc. R. Soc. London, Ser. A **246**, 215 (1953).
[51] M. J. Seaton, Comput. Phys. Commun. **25**, 87 (1982).
[52] W. Weizel, in *Handbuch der Experimentalphysik*, edited by W. Wein and F. Harms (Akademische, Leipzig, Supplement, 1931), Vol. 1, p. 42.
[53] Ch. Jungen and O. Atabek, J. Chem. Phys. **66**, 5584 (1977).
[54] M. Barat and W. Lichten, Phys. Rev. A **6**, 211 (1972).
[55] R. R. Lucchese and V. McKoy, Phys. Rev. A **24**, 770 (1981).
[56] L. Collins and D. Robb (results tabulated in Ref. 54, and quoted as unpublished work); see also W. D. Robb and L. A. Collins, Phys. Rev. **22**, 2474 (1980).
[57] H. Takagi and H. Nakamura, Phys. Rev. A **27**, 691 (1983); J. Phys. B **13**, 2619 (1980).
[58] B. R. Tambe and B. Ritchie, J. Chem. Phys. **68**, 3595 (1978).
[59] A. Temkin and K. V. Vasavada, Phys. Rev. **160**, 109 (1967); A. Temkin, K. V. Vasavada, E. S. Chang, and A. Silver, *ibid.* **186**, 57 (1969).
[60] Ch. Jungen and D. Dill, J. Chem. Phys. **73**, 3338 (1980).
[61] Ch. Jungen, I. Dabrowski, G. Herzberg, and M. Vervloet, J. Chem. Phys. **93**, 2289 (1990).
[62] However, we were able to obtain the $b\,^3\Sigma_u^+$ repulsive state from $R=1.2-2.2\ a_0$, by calculating the eigenphases explicitly to as low as -8.0 eV below threshold. Table III gives its total energy at $R=2.0\ a_0$.
[63] E. E. Eyler, R. C. Short, and F. M. Pipkin, Phys. Rev. Lett. **56**, 2602 (1986).
[64] H. Lefebvre-Brion and C. M. Moser, J. Mol. Spectrosc. **15**, 211 (1965).
[65] W. J. Hunt and W. A. Goddard III, Chem. Phys. Lett. **3**, 414 (1969).
[66] S. Rothenberg and E. R. Davidson, J. Chem. Phys. **45**, 2560 (1966).
[67] W. Kolos and L. Wolniewicz, J. Chem. Phys. **48**, 3672 (1968).
[68] W. Kolos, J. Mol. Spectrosc. **62**, 429 (1976).
[69] W. Kolos and L. Wolniewicz, J. Chem. Phys. **43**, 2429 (1965).
[70] W. Kolos and J. Rychlewski, J. Mol. Spectrosc. **62**, 109 (1976).
[71] L. Wolniewicz and K. Dressler, J. Chem. Phys. **88**, 3861 (1988).
[72] I. Dabrowski and G. Herzberg, Can. J. Phys. **52**, 1110 (1974).